Supporting Information

Charge Transport of Phosphonate Self-assembled Monolayers across Eutectic Gallium–Indium-based Molecular Junctions

Shi Huang,†[a] Qianqian Guo,†[a] Jiancong Ni,[a,b] Zhenyu Lin*[c] and Xiaoping Chen*[a,b]

Table of Contents

S1. Atomic Force Microscope (AFM) characterization of ITO substrates

An atomic force microscope (FM-nanoview 6800, Feishiman Co., Ltd., Suzhou, China) at a tapping mode was used to characterize the surface rms roughness of the ITO substrates. Figure S1 shows the AFM image over a size of 5×5 um^2.

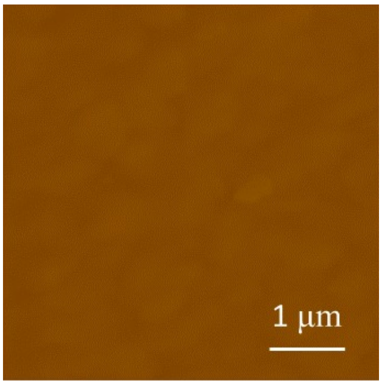

Figure S1. The AFM image of 30 nm ITO on polished Si wafer surface with a size of 5×5 um^2.

S2. Water Contact Angle Characterization for SAMs on ITO Substrates

The static water contact angle was characterized using the same camara setup as EGaIn electrical J(V) characterization. 10 uL deionized water was dropped on the ITO-$PO_3(CH_2)_nH$ surface to record the water contact angle as shown in Figure S2.

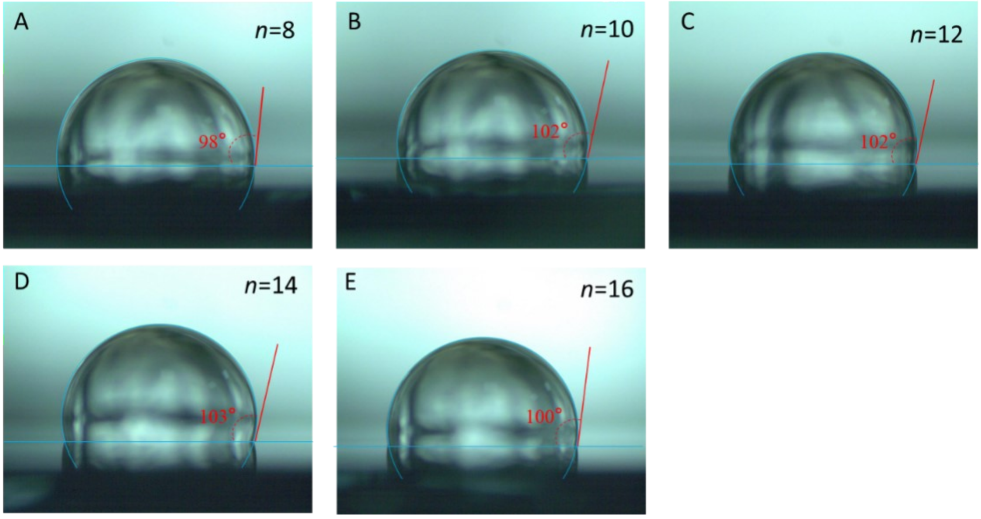

Figure S2. The photos taken from the water contact angle experiment for ITO-$PO_3(CH_2)_nH$ SAMs.

S3. XPS Characterization of SAMs on ITO Substrates

Figures S3-S6 show the C 1*s*, P 2*p*, O 1*s*, and In 3*d* spectra obtained from The angle-resolved X-ray photoelectron spectroscopy (ARXPS) characterization at the take-off angles of (θ) of 90°and 40°, respectively.

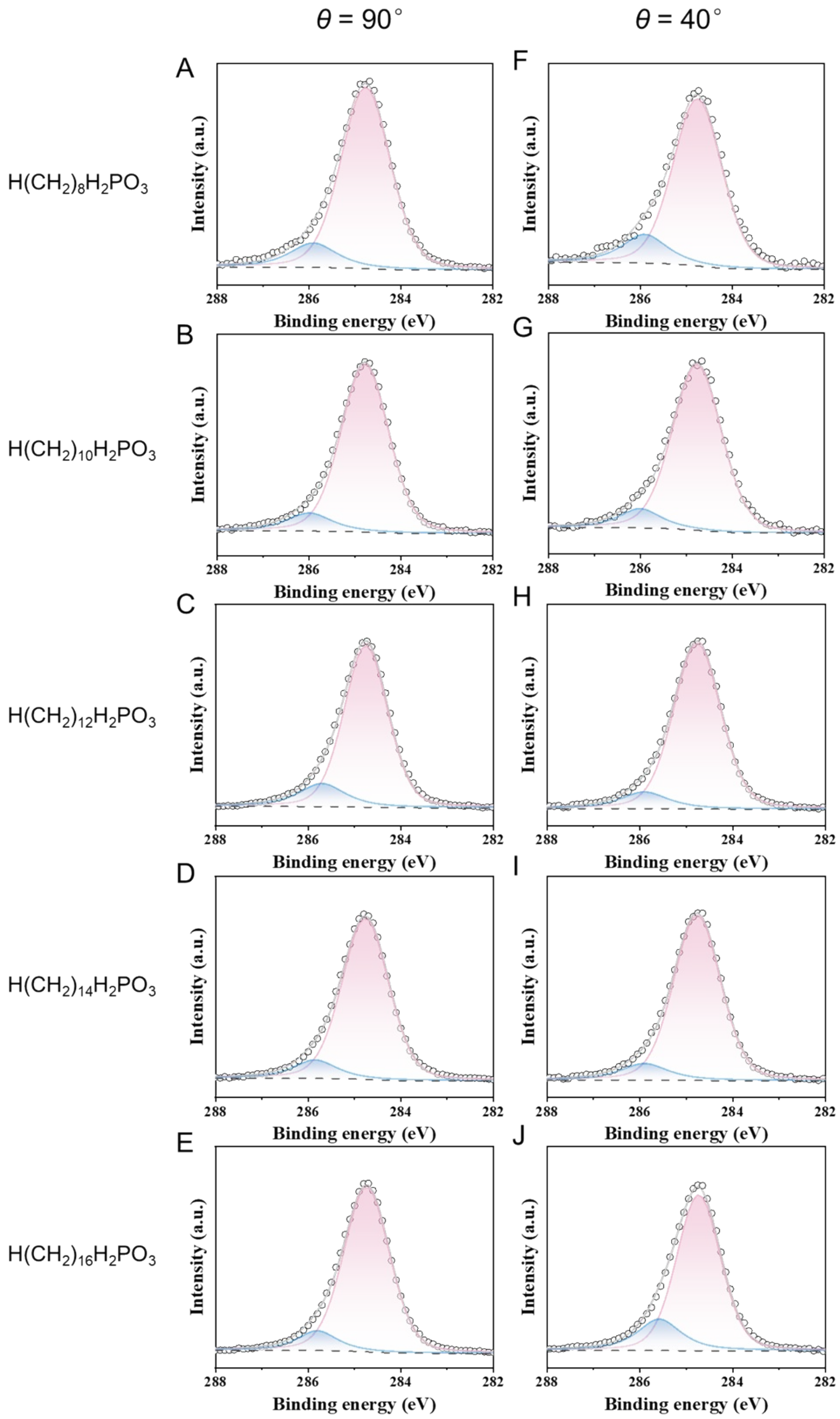

Figure S3. (A-E) C 1*s* peaks of ITO-$PO_3(CH_2)_nH$ SAMs at the take-off angle θ of 90^o, respectively; (F-J) C 1*s* peaks of ITO-$PO_3(CH_2)_nH$ SAMs at the θ of 40^o, respectively.

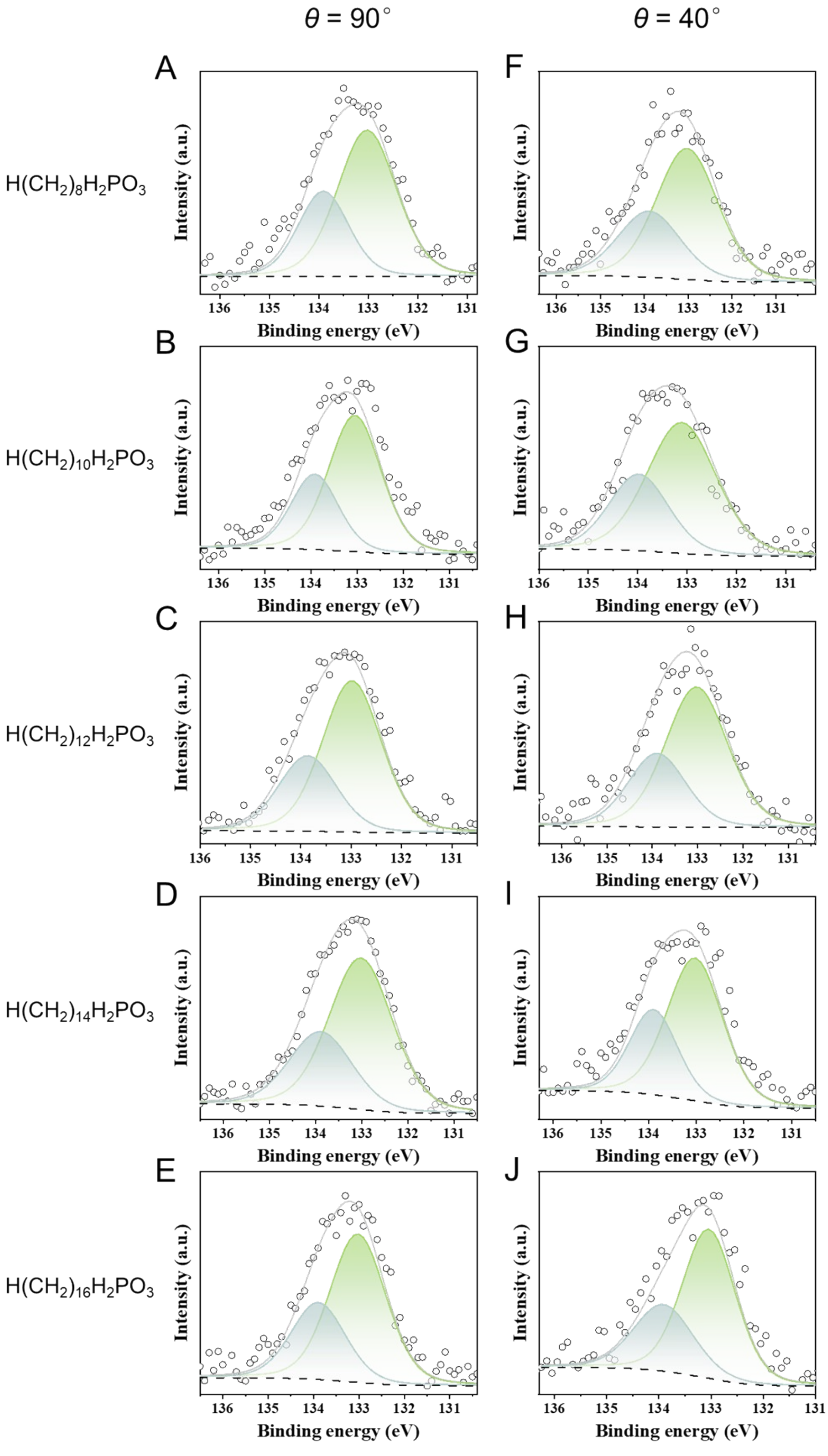

Figure S4. (A-E) P 2*p* spectra of ITO-$PO_3(CH_2)_nH$ SAMs at the θ of 90°, respectively; (F-J) P 2*p* spectra of ITO-$PO_3(CH_2)_nH$ SAMs at the θ of 40°, respectively.

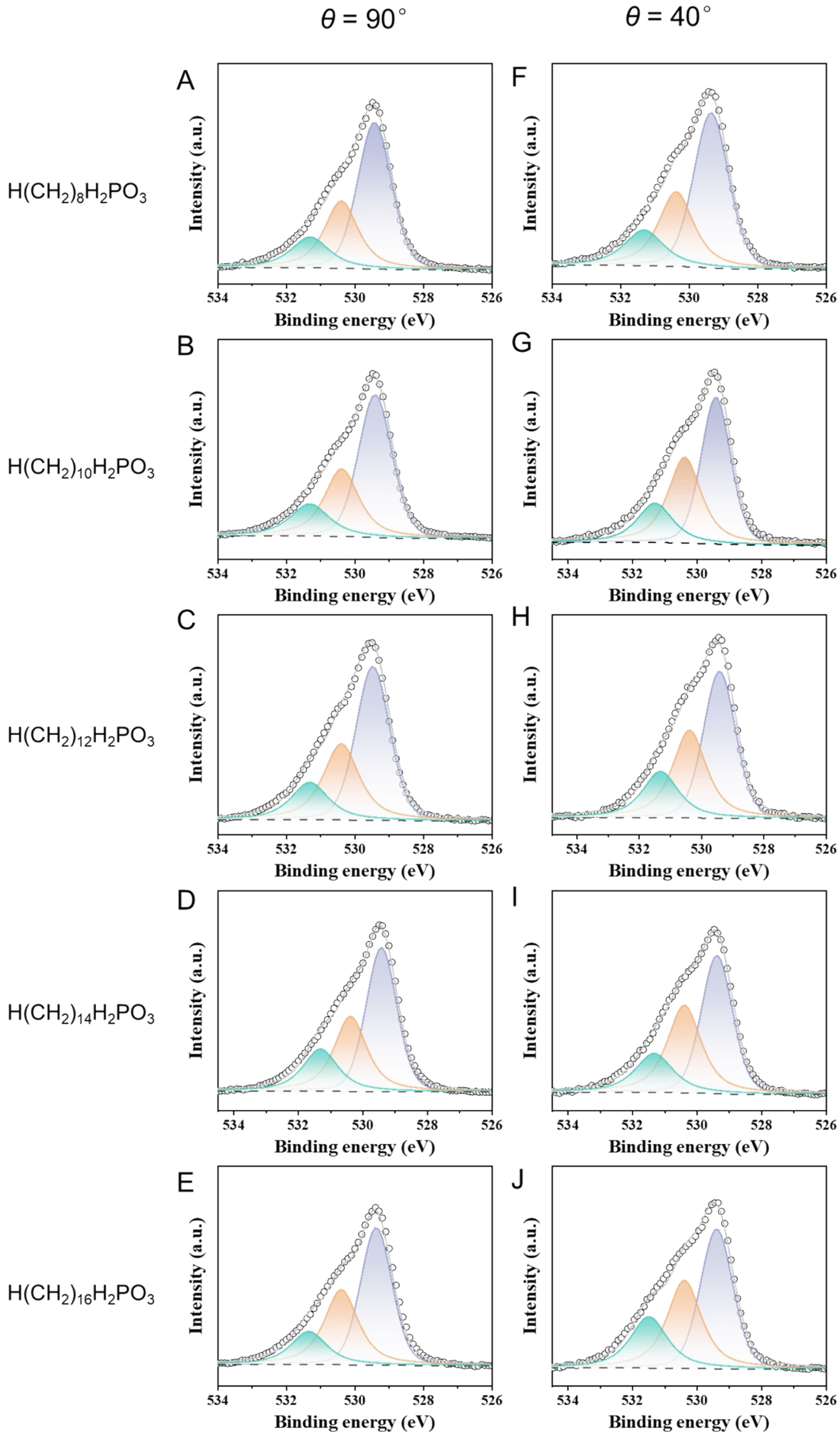

Figure S5. (A-E) O 1*s* spectra of ITO-$PO_3(CH_2)_nH$ SAMs at the θ of 90°, respectively; (F-J) O 1*s* spectra of ITO-$PO_3(CH_2)_nH$ SAMs at the θ of 40°, respectively.

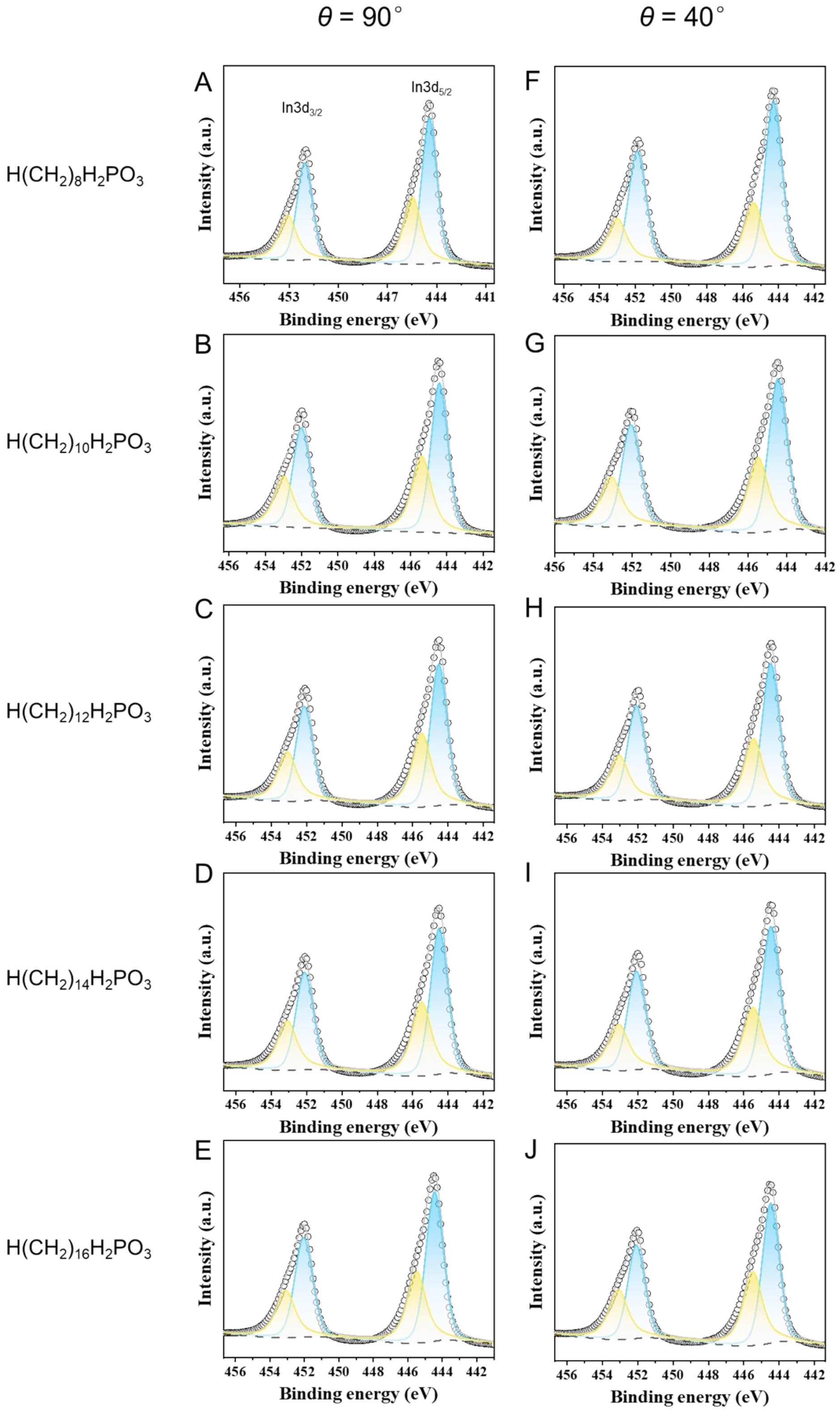

Figure S6. (A-E) In 3*d* spectra of ITO-$PO_3(CH_2)_nH$ SAMs at the *θ* of 90°, respectively; (F-J) In 3*d* spectra of ITO-$PO_3(CH_2)_nH$ SAMs at the *θ* of 40°, respectively.

S4. UPS characterization of SAMs on ITO Substrates

Figure S7 shows the kinetic energy of photoelectrons from the secondary cutoff spectra were used for the determination of the work function of substrate (Φ_{SAM}, in eV) and the binding energy from the valence band provided the HOMO onset (ΔE_{HOMO}, in eV). The intersections at the tangent of the peak and the linear extrapolation of the lower kinetic energy or lower binding energy indicate the Φ_{SAM} and ΔE_{HOMO} values, respectively.

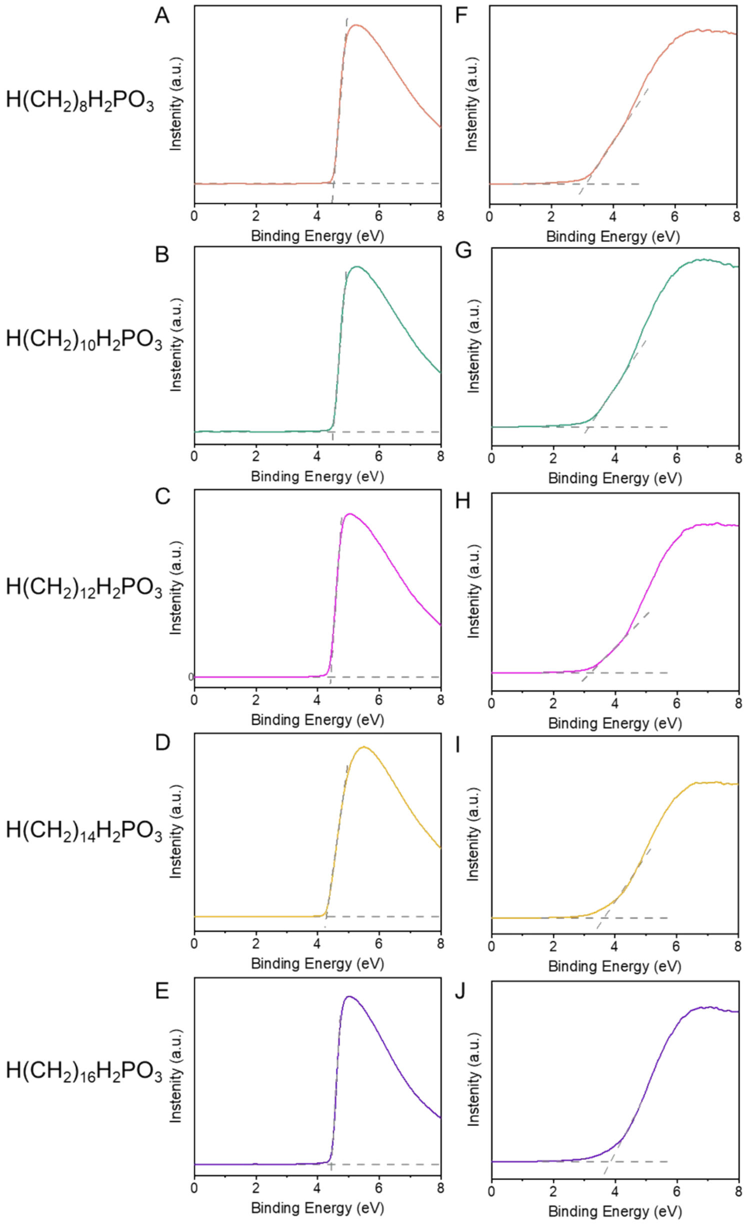

Figure S7. Ultraviolet photoelectron spectroscopies of the ITO-$PO_3(CH_2)_nH$ SAMs. (A-E) Secondary electron cut-off spectra of the SAMs. (F-J) Valence band spectra of the SAMs. The cross-section of the dashed lines indicates work function and HOMO onset values.

S5. Electrical J(V) characterization of con-shaped EGaIn junctions

Figure S8 and Table S1 summarize the electrical *J*(V) characterization results for ITO-$PO_3(CH_2)_nH//GaO_x/EGaIn$ junctions.

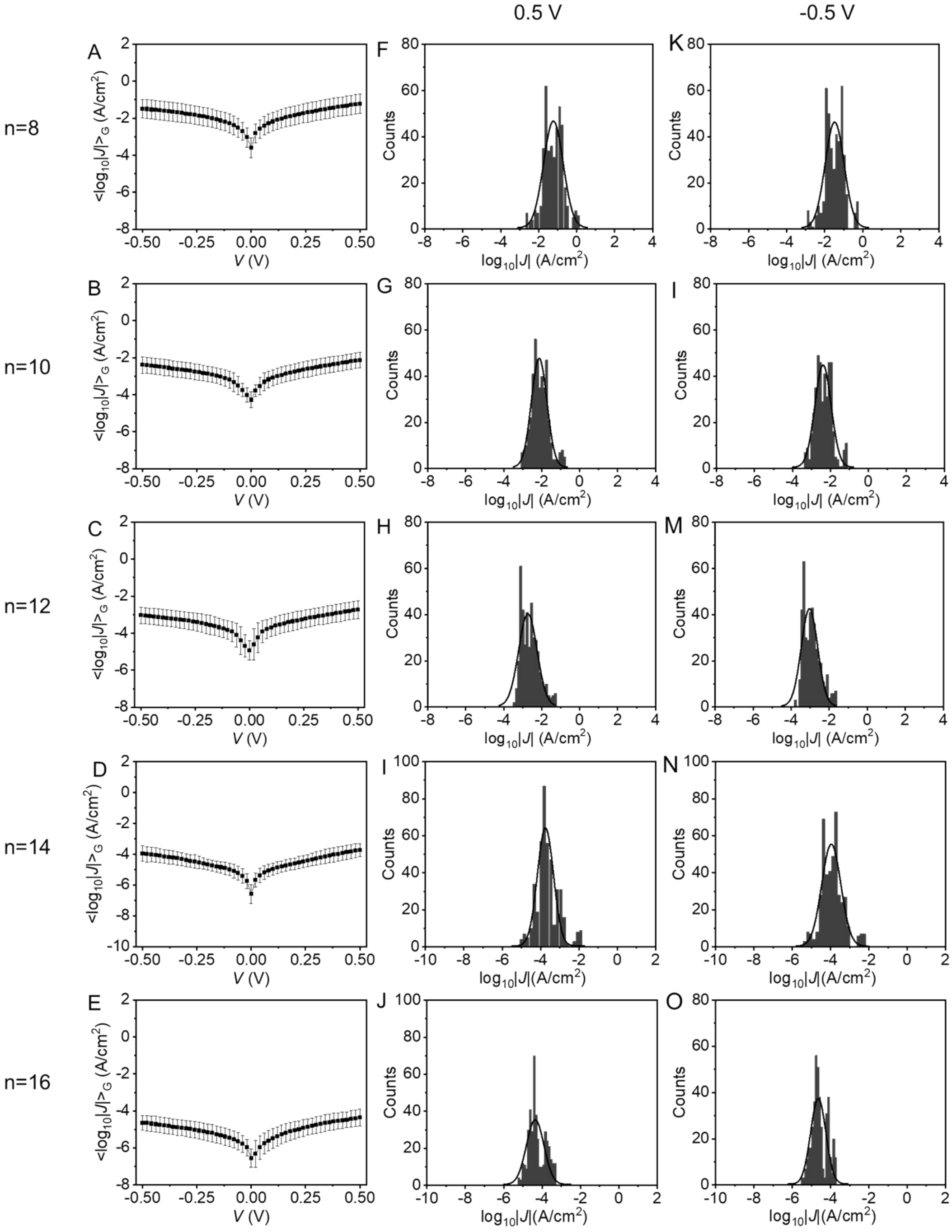

Figure S8. $\langle\log_{10}|J|\rangle_G$ *vs*. applied bias *V* curves (A-E) and histogram of $\log_{10}|J|$ with a Gaussian fit (black lines) at +0.5 V (F-J) and -0.5 V (K-O) for ITO-$PO_3(CH_2)_nH//GaO_x/EGaIn$ junctions; The bold symbol in the *J*(V) curves represent$\langle\log_{10}|J|\rangle_G$ at each bias, the error bars represent the $\sigma_{\log,G}$, and the black line in the histogram are the result of Gaussian fitting.

Table S1. Summary of *J*(V) results of junctions of ITO-$PO_3(CH_2)_nH$//GaO_x/EGaIn

n	No. of junctions	No. of shorts/unstable junctions [a]	No. of Traces [b]	Yield (%) [c]	$\langle \log_{10}\lvert J\rvert \rangle_{G(-0.5\ V)}(\pm\sigma_{\log,G})$	$\langle \log_{10}\lvert J\rvert \rangle_{G(0.5\ V)}(\pm\sigma_{\log,G})$
8	29	7	426	81	-1.23±0.52	-1.48±0.50
10	26	4	440	85	-2.14±0.41	-2.39±0.43
12	24	3	420	88	-2.73±0.48	-3.04±0.43
14	25	3	439	88	-3.75±0.42	-3.96±0.50
16	23	3	417	87	-4.36±0.46	-4.64±0.40

[a] A short junction is that during the process of recording *J*(V) scans, the value of *J* exceeds the detection limit of this instrument (100 mA/cm^2); an unstable junction is that when recording *J*(V) scans, the *J* suddenly increases by three orders of magnitude compared to the average value of *J*.

[b] The number of traces refers to the total number of traces from all junctions that are non-shorting and stable, normally 20 traces were recorded for each junction.

[c] Yield of non-shorting junctions is defined as the number of non-shorting junctions over the total number of junctions.

S6. Impedance characterization of EGaIn junctions

Figure S9 summarizes the Nyquist plots, Bode plots, and phase plots of different ITO-$PO_3(CH_2)_nH$//GaO_x/EGaIn junctions. The fitted results of R_{SAM}, R_C, and C_{SAM} are listed in Table S2.

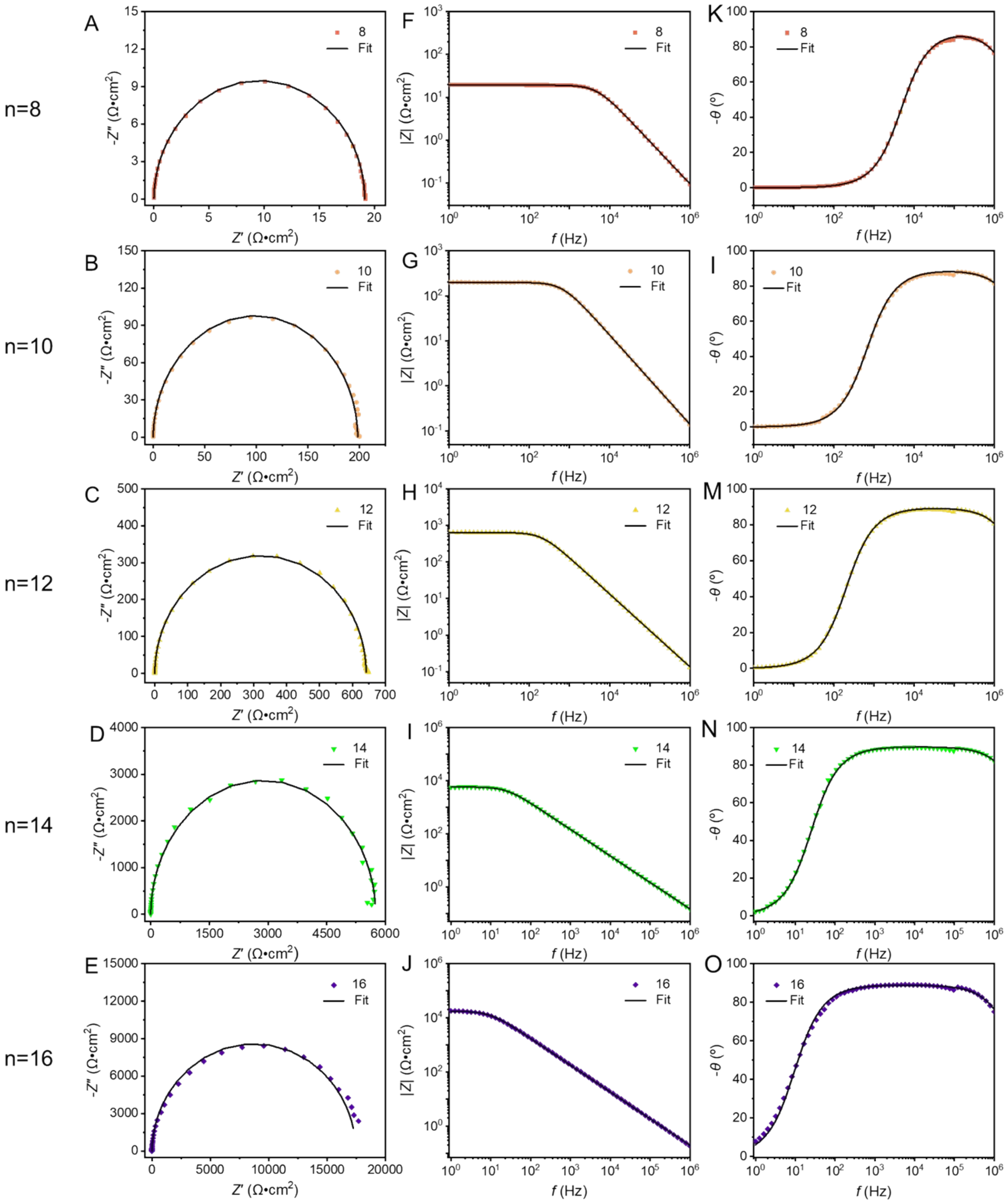

Figure S9. Nyquist plots (A-E), Bode plots (F-J), and phase plots (K-O) of ITO-$PO_3(CH_2)_nH$//GaO_x/EGaIn junctions at an AC bias of 30 mV from impedance characterization.

Table S2. Summary of impedance results of ITO-$PO_3(CH_2)_nH$//GaO_x/EGaIn junctions

n	$\log_{10}R_{SAM}$ ($\Omega\cdot cm^2$)	R_C ($m\Omega\cdot cm^2$)	C_{SAM} ($\mu F/cm^2$)	ε_r	n_{CPE}
8	1.28±0.05	19.47±1.36	1.72±0.13	2.46±0.19	0.98±0.03
10	2.31±0.01	17.25±1.08	1.41±0.13	2.28±0.21	0.98±0.01
12	2.80±0.19	20.90±0.01	1.25±0.02	2.48±0.00	0.99±0.00
14	3.85±0.06	19.69±0.75	1.11±0.01	2.34±0.03	0.99±0.00
16	4.26±0.05	23.40±2.36	1.09±0.01	2.60±0.02	0.98±0.01